

Two-dimensional array of microtraps with atomic shift register on a chip

S. Whitlock,* R. Gerritsma, T. Fernholz, and R. J. C. Spreeuw

Van der Waals-Zeeman Institute, University of Amsterdam, Amsterdam, The Netherlands.

(Dated: March 15, 2019)

Arrays of trapped atoms are the ideal starting point for developing registers comprising large numbers of physical qubits for processing quantum information [1, 2]. One very promising approach involves neutral atom traps produced on microfabricated devices known as atom chips [3, 4], as almost arbitrary trap configurations can be realised in a robust and compact package. Until now, however, atom chip experiments have focused on small systems incorporating single or only a few individual traps. In this letter we report experiments on a vast two-dimensional array of trapped ultracold atom clouds prepared using a simple magnetic-film atom chip. We are able to load atoms into hundreds of tightly confining and optically resolved array sites. We then cool the individual atom clouds in parallel to the critical temperature required for quantum degeneracy. Finally, we shuttle atoms across the film surface utilising the atom chip as an atomic shift register.

Of central importance in the quest for a quantum computer is the issue of scalability. In the *trapped-ion* approach for example, microfabricated-chip traps [5] have recently been able to accommodate several ions [6, 7] and shuttle them between different zones [8]. *Neutral atoms* on the other hand possess the significant advantage of an intrinsically weaker interaction with the environment, yet are routinely manipulated using optical and magnetic trapping techniques. So far, the primary tool used to create registers of neutral atoms has been the optical lattice, which allows near-perfect arrays of atoms with typical separations of half the optical wavelength [9]; however addressing and locally manipulating atoms on this length-scale remains a serious challenge. This has motivated the development and use of large-period optical lattices [10, 11] or patterned loading techniques [12], as well as addressable arrays of optical traps produced using holographic techniques [13] or micro-lens arrays [14].

Magnetic microtraps integrated on atom chips [15, 16] are a promising alternative to these optical approaches. An atom chip typically consists of a microscopic pattern of wires (micro-electromagnets) or permanent magnets [17, 18, 19] arranged on a substrate as to produce tailor-made magnetic potentials for ultracold atoms. Qubits encoded in the ground-state hyperfine levels of the trapped atoms offer exceptionally long coherence times [20], and quantum-logic gates could be implemented via controlled collisions [21] or by long-range in-

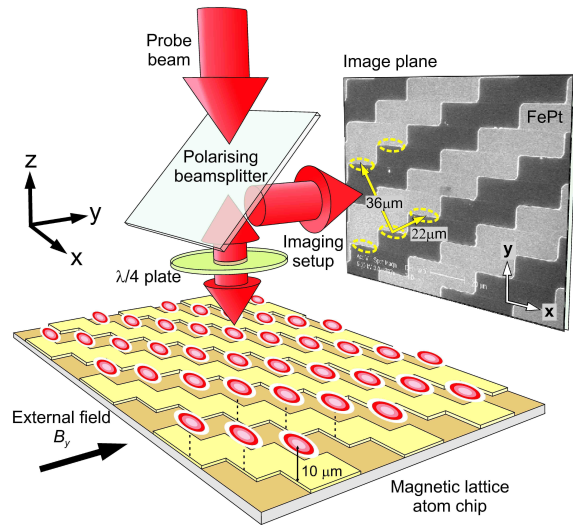


FIG. 1: **Magnetic lattice atom chip and experimental setup.** The experiments are performed using a FePt magnetic film, lithographically patterned with a two-dimensional lattice with periods of $22 \mu\text{m}$ and $36 \mu\text{m}$ and coated with a reflective gold layer. The film is uniformly magnetised along z and combined with an external field B_y to create a vast array of magnetic microtraps for atoms positioned $10 \mu\text{m}$ from the film surface. For detection, the trapped atoms are illuminated by a retro-reflected probe laser beam which is partly absorbed by the atoms and imaged onto a CCD camera for analysis. Projected on the backplane of the figure is a microscope image of the FePt film with a few trap positions indicated by yellow ellipses.

teractions using laser excited Rydberg states [22]. With established micro/nano-fabrication techniques it is then feasible to scale-up and integrate many microtraps on a single chip. As we show here, magnetic-film atom chips are particularly ideal for this purpose, allowing the integration of hundreds of tightly confining traps in custom-designed and optically resolvable microtrap arrays [23, 24].

At the core of our experiment (Fig. 1) is an atom chip (for design and fabrication details see ref. [23]) which incorporates an 300-nm thick FePt film, patterned using optical lithography, then gold-coated and magnetised in the direction perpendicular to the film surface ($M_z = 670 \text{ kA/m}$). Combined with an external field ($B_y = 22.5 \text{ G}$), this simple setup produces a two-dimensional array of magnetic field minima (magnetic lattice), which is used to trap ultracold ^{87}Rb atoms in the $|F=2, m_F=2\rangle$ state. Each trap is produced $10 \mu\text{m}$ from

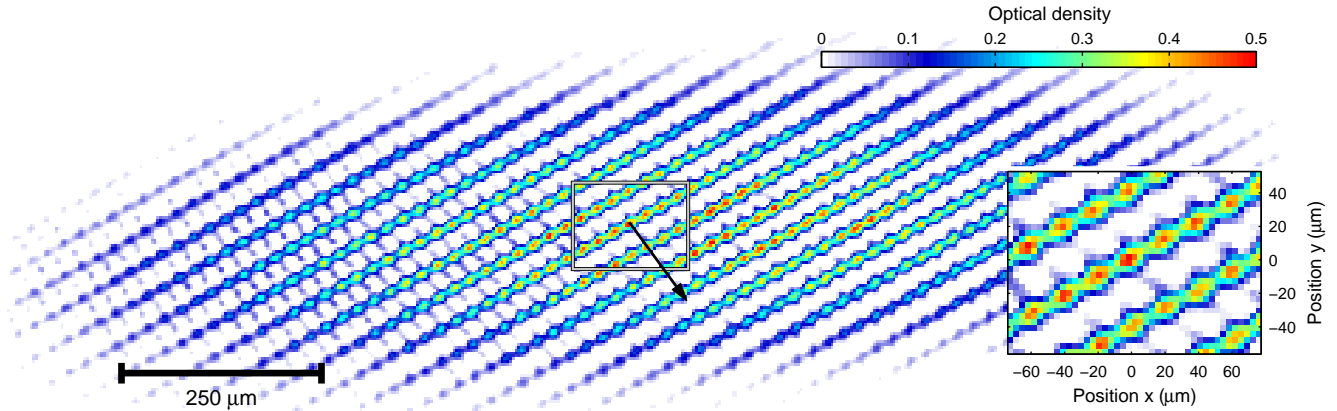


FIG. 2: **Loaded array of magnetic microtraps.** A two-dimensional absorption image of the atomic distribution (shown in false-colour) after transfer to the magnetic lattice. The optical resolution is approximately $7 \mu\text{m}$. The inset shows a magnified region of the central part of the array as indicated by the outlined box. Atoms populate more than 500 array sites over a region of $1.4 \times 0.4 \text{ mm}^2$ of the chip surface; the scale bar corresponds to a distance of $250 \mu\text{m}$. The solid arrow indicates the direction of transport for the atomic shift register experiment (Fig. 4).

the surface and provides tight harmonic confinement to the atoms (with trapping frequencies $\omega_{\parallel}/2\pi = 5.5 \text{ kHz}$ and $\omega_{\perp}/2\pi = 13.4 \text{ kHz}$ in the axial and transverse directions respectively). The distances between neighbouring traps are $22 \mu\text{m}$ and $36 \mu\text{m}$ ($1250 \text{ traps}/\text{mm}^2$), chosen to facilitate optical addressing. The barriers between traps, the trapping frequencies and the trap positions are precisely controlled through the external field. We believe magnetic-film atom chips are best suited for high-density integration, as for example, an equivalent potential produced using currents through micron-sized gold wires would require a power dissipation of $\sim 30 \text{ W}/\text{mm}^2$.

We first describe the loading of the microtrap array. A cloud of ^{87}Rb atoms is collected and cooled in a mirror-magneto-optical-trap and then transferred to a single magnetic trap created by a current-carrying wire and the external field [15]. A two-dimensional view of the atomic distribution is obtained using reflective resonant absorption imaging (Fig. 1). The cloud contains $N = 1 \times 10^6$ atoms at a temperature of $\sim 30 \mu\text{K}$ before it is transferred to the film surface by ramping off the wire current. The atom cloud first becomes corrugated as the trap merges with the field of the lattice, until for zero wire current the atoms are confined in the microtrap array alone (Fig. 2). We determine the number of atoms in each trap by integrating the absorption over each unit cell. During merging, the atom cloud expands over an area of $\sim 1.4 \times 0.4 \text{ mm}^2$, populating more than 500 traps, each with $N > 200$ and up to 2500 atoms, showing it is possible to transfer atoms from a single magnetic trap to hundreds of microtraps. After loading, we observe atom loss over two characteristic time-scales: minor initial loss over the first 100 ms, caused by residual evaporation of

atoms over the potential barriers, then background loss, occurring with a time-constant of around 2 s.

For storing quantum information, it is desired to initialise the register to a well-defined state with negligible thermal excitations. We have cooled all atom clouds simultaneously by forced evaporation using a two-part radio-frequency (rf) sweep with a duration of 235 ms (see Methods). Radio-frequency spectroscopy [19] and density-dependent decay rates are then used to characterise more than 150 microtraps near the center of the array (Fig. 3).

Radio-frequency spectroscopy is performed at several intervals during the evaporation sweep, and analysed independently for each microtrap to determine the cloud temperature T and the magnetic field strength at the trap minimum (Fig. 3a). Using this technique we can perform hundreds of simultaneous measurements on individual atom clouds within the microtrap array. Before evaporation, we find the cloud temperatures are nearly equal for all traps (red-squares in Fig. 3c) with $\langle T \rangle = 43 \pm 4(3) \mu\text{K}$ (most-likely constrained by the trap depth of around $400 \mu\text{K}$). Here we quote the *rms* spread among the traps with the estimated contribution from statistical uncertainties per trap in parentheses. The spread of the trap minima has also been measured to be $46(4.6) \text{ mG rms}$. During evaporation (down to temperatures around $3 \mu\text{K}$), we find high cooling rates and high evaporation efficiencies ($d(\ln T)/d(\ln N)$ between 1.2 and 1.7), attributed to the extremely high elastic collision rates present in our stiff traps (between $2500 - 5000 \text{ s}^{-1}$), despite the relatively small number of atoms per array site.

Towards the end of the evaporation sweep we mea-

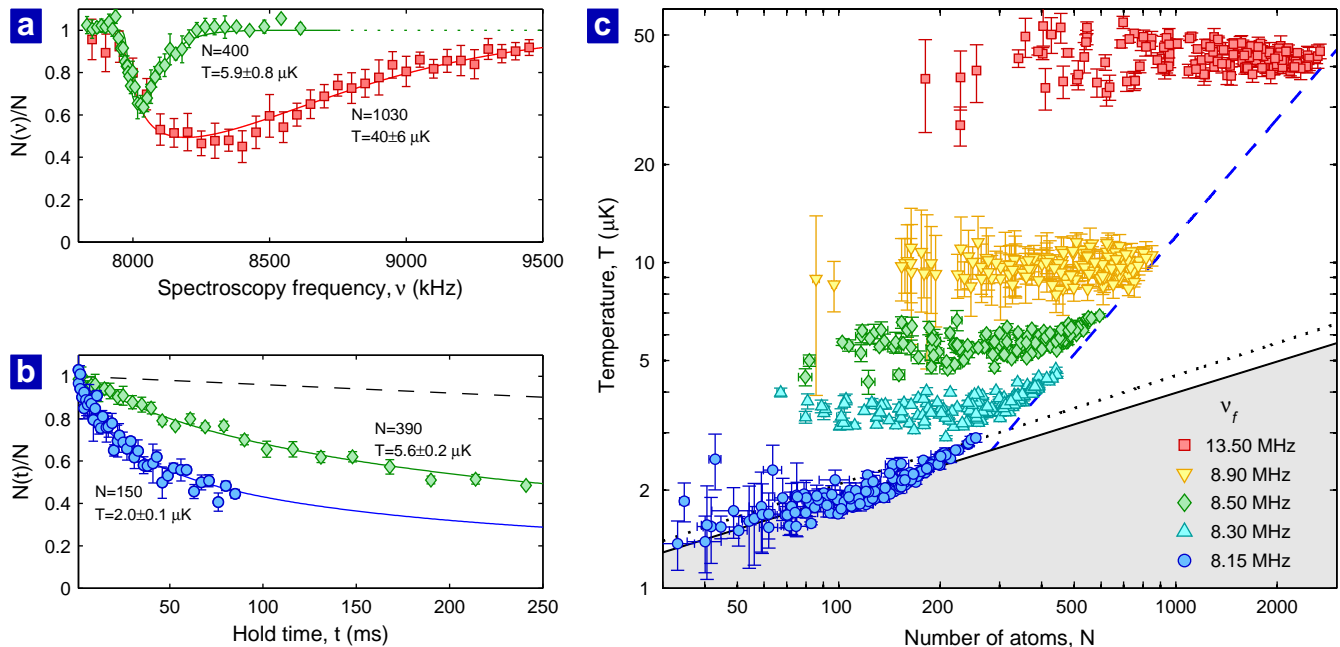


FIG. 3: **Radio-frequency evaporative cooling and site-resolved thermometry.** Forced radio-frequency (rf) evaporation is used to cool the individual atom clouds to the critical temperature for quantum degeneracy. Site-resolved rf spectroscopy and three-body decay measurements are performed to determine the distribution of cloud temperatures. (a) Two representative rf spectra and fits (solid lines) for one selected site for final evaporation frequencies of $\nu_f = 13.5$ MHz (red squares) and $\nu_f = 8.50$ MHz (green diamonds), with fitted values for N and T labelled. (b) Two representative three-body decay curves and fits (solid lines) for the same array site as in (a) for $\nu_f = 8.50$ MHz and $\nu_f = 8.15$ MHz (blue circles). The dashed line indicates the expected loss due to background vapour collisions with $\tau = 2$ s. (c) The full set of data (N, T), for >150 array sites and five different final evaporation frequencies. The error-bars represent statistical uncertainties estimated from several repetitions of the experiment. The blue dashed line indicates a constant evaporation efficiency of $d(\ln T)/d(\ln N) = 1.2$ calculated for one site. The dotted line marks the Bose-Einstein condensation transition (degeneracy temperature) in the thermodynamic limit neglecting interactions. The numerically calculated boundary to the grey region is for a constant phase-space-density of $\rho_0 = 2.612$, corresponding to the onset of Bose-Einstein condensation including the effects of finite atom number and interactions (see Methods section).

sure high decay rates due to three-body recombination loss [25, 26] ($\gamma > 20 \text{ s}^{-1}$), which can be used to characterise the array (Fig. 3b). Using a mean-field description of the atomic distributions we predict decay-curves as a function of N and T (see Methods). Fitting this model to the measurements taken after the evaporation sweep indicates peak atomic densities $> 1 \times 10^{15} \text{ cm}^{-3}$ and temperatures around $\langle T \rangle = 2.0 \pm 0.3 \mu\text{K}$ (blue-circles in Fig. 3c) corresponding to 2.6 and 7.1 mean vibrational quanta in the transverse and axial modes respectively. Each cloud is smaller than the optical wavelength (Lamb-Dicke regime), with *rms* position spreads of $0.17 \pm 0.01 \mu\text{m}$ and $0.4 \pm 0.03 \mu\text{m}$. Our data also indicates 50% of the clouds have a phase-space-density ($\rho > \rho_0 \simeq 2.612$) corresponding to the onset of Bose-Einstein condensation. Around this point the cooling efficiency sharply decreases which we attribute to increased three-body decay for partially condensed clouds causing a “relaxation explosion” [27]. This effect may be circumvented in the future by trapping fewer atoms per site or by using the weaker-confined $|F = 1, m_F = -1\rangle$ state which also has a lower three-

body-decay coefficient [25]. Through rf-evaporation and site-resolved measurements of three-body recombination rates we have shown it is possible to efficiently cool atoms in many array sites to the critical temperature for quantum degeneracy.

In addition to trapping and cooling the atom clouds we have transported the atoms across the atom chip. This atomic shift register is a parallelised version of atomic [3] and molecular [28] conveyor belts and is the cold-atom analog of an electronic CCD (charge-coupled device). Rotating the external magnetic field continuously displaces the traps [29](see Methods), shifting the array along one lattice direction as shown in Fig. 4. We have computed the optimised field components (Fig. 4a) required to keep the traps at a fixed height of $10 \mu\text{m}$ and with the field minima at a constant 3.23 G, chosen to prevent dephasing of our prospective qubits, as the differential Zeeman shift vanishes at this field strength [20]. In the experiment we first cool the atom clouds to a temperature of $\sim 10 \mu\text{K}$ and then linearly ramp between six settings of the external field per period, in 6×3 ms inter-

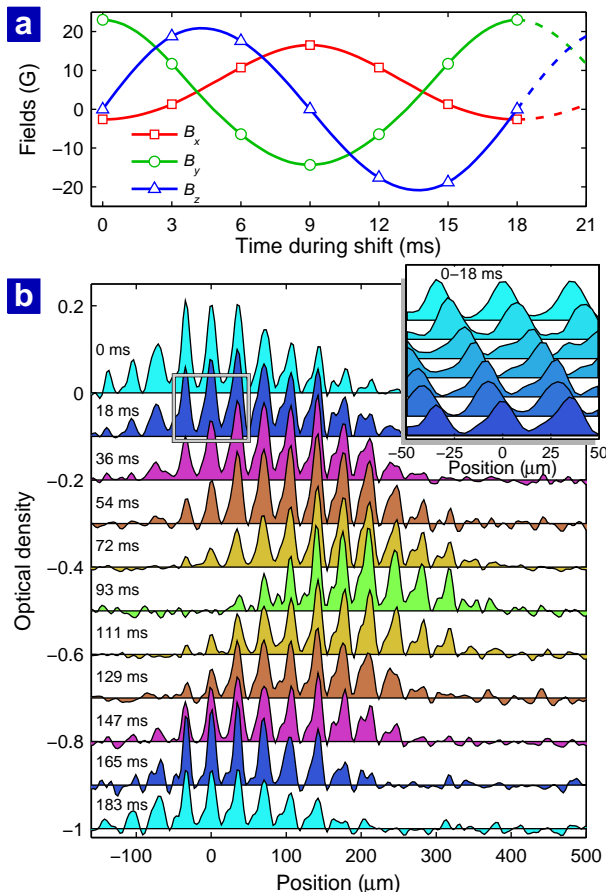


FIG. 4: **Transport of atoms over the chip surface: atomic shift register.** An external homogeneous magnetic field with rotating orientation smoothly shuttles the array of atom clouds in one direction and back. **(a)** Calculated optimal time-sequence for the external magnetic fields B_x (red), B_y (green) and B_z (blue) applied to carry-out a single cycle shift operation. The field values shown as open symbols are applied in the experiment and interpolated by linear field ramps. **(b)** Line-scans of optical density images along the shifting direction (arrow indicated in Fig. 2). Data for an integer number of shift cycles are shown, each with a vertical offset of -0.1 for clarity. A total of five shifts, each covering one lattice period, and five in the reverse direction to the original position are shown. The full sequence takes 183 ms and the atoms are transported over a distance of $360 \mu\text{m}$. The inset shows intermediate steps within the first shift cycle for each 3 ms interval.

vals. By repeating the shifting sequence we have transported the atoms over a round-trip distance of $360 \mu\text{m}$, with five shifts in the $(2, -3)$ direction (Fig. 2) followed by five reverse shifts (Fig. 4b). During the experiment we observe about 40% atom loss, which is higher than the background loss rate and becomes more severe for shorter shifting intervals. We attribute this to the finite time-response of our electromagnetic coils which fail to accurately reproduce the optimised fields. We expect

integrating additional wires on the chip to produce time-dependent control fields for this purpose will be a valuable addition to our design. The demonstrated ability to shuttle atoms across the chip is an important ingredient for a scalable architecture for quantum computing and is an inherent feature of our magnetic-film atom chip.

To conclude, we have reported experiments on a two-dimensional array of ultracold atom clouds prepared near the surface of a magnetic film atom chip. This promising new architecture for scalable quantum information processing combines optically-resolved trap separations with tight magnetic confinement. We have loaded atoms into more than 500 array sites and performed rf evaporative cooling of these atom clouds to the quantum degeneracy temperature. In the process we have demonstrated preparation, cooling, detection and analysis of hundreds of atom clouds in parallel; highlighting magnetic micro-trap arrays as a unique experimental test bed for studying ultracold atomic systems and quantum matter. Using existing microfabrication technology we anticipate further scaling, to lattice dimensions of a few micrometers, in order to accommodate thousands of individual atomic qubits. Finally an atomic shift register is used for parallel transport of atoms across the chip surface, allowing the separation of storage, interaction and readout areas of a future, fully integrated device.

Methods

Radio-frequency evaporation and spectroscopy

Sweeping the radio frequency from high to low frequency continuously couples the more energetic atoms to untrapped Zeeman states (which subsequently leave the traps) while the remaining atoms rethermalise to lower temperatures. In our experiments (Fig. 2,3) the field minima of the potentials is around $11.41 \pm 0.05 \text{ G}$ corresponding to a Zeeman energy splitting of $\sim 7.99 \text{ MHz}$. We first ramp from 13.5 MHz to 8.5 MHz in 200 ms (corresponding to effective trap depths of around $48 \mu\text{K}$), then from 8.5 MHz to 8.15 MHz in 35 ms ($15 \mu\text{K}$). We characterise the system using techniques which allow for parallel analysis of each atom cloud and do not require the traps to be switched off. In rf-spectroscopy, a rf field is pulsed for $\sim 1 \text{ ms}$ with a variable frequency to selectively outcouple atoms depending on their energy. We record an absorption image to determine the number of atoms in each site and repeat the experimental cycle for each value of the spectroscopy-frequency to construct a collection of energy distributions (one for each site (Fig. 3a)). We fit a model to the measured spectra [19] based on the calculated atomic distributions (see below) to determine the cloud temperatures and the magnetic field strength at the trap minima. For the transport experiments of Fig. 4 we first evaporate at a bottom field of 11.41 then ramp the fields to $\sim 3.23 \text{ G}$ to carry out the shifting sequence.

Mean-field model for atomic distributions

The data is interpreted using a self-consistent mean-field model for the atomic density distributions for a thermal fraction, $n_{\text{th}}(r)$ and a Bose-condensed fraction, $n_0(r)$, for a given

N and T . The model accounts for quantum statistics and the effect of interactions for both the thermal and condensed components but neglects the kinetic energy of the condensed fraction via the Thomas-Fermi approximation. We approximate the trap potential as isotropic $V(r) = m\bar{\omega}^2 r^2/2$ with mean trap frequency $\bar{\omega} = (\omega_{\parallel}\omega_{\perp}^2)^{1/3}$, and iteratively solve the following set of equations:

$$\begin{aligned} n_0(r) &= \max \left[\frac{1}{g} (\mu - V(r) - 2g n_{\text{th}}(r)), 0 \right] \\ n_{\text{th}}(r) &= \frac{1}{\Lambda^3} g_{3/2} \left[e^{[\mu - V_{\text{eff}}(r)]/k_B T} \right] \\ V_{\text{eff}}(r) &= V(r) + 2g (n_{\text{th}}(r) + n_0(r)) \end{aligned} \quad (1)$$

with $N = \int (n_0 + n_{\text{th}}) d^3 r$ and using the standard definitions: g is the coupling strength, Λ is the thermal de Broglie wavelength, $g_n(z)$ is the polylogarithm function and μ is the chemical potential. The numerical solutions are then used to predict the spectral energy distribution and three-body decay rate (see below) for fitting data as a function of N and T over the full range probed in our experiments. The solutions are also used to numerically determine the line $n(0)\Lambda^3 = 2.612$ in Fig. 3.

Thermometry by three-body decay

For low temperatures we observe rapid density-dependent loss due to three-body recombination which can be accurately measured to characterise the array [25, 26]. A collection of decay curves is obtained by holding the atoms for a variable duration (one value per experimental cycle) before taking an absorption image and integrating the number of atoms in each site. During the hold time we apply a radio-frequency “shield” tuned to the final evaporation frequency ν_f to limit the trap depth and prevent heating. Three-body decay curves are modelled with the following differential equation:

$$\begin{aligned} \dot{N} &= -L \left[\int n_0^3 d^3 r + 9 \int n_0^2 n_{\text{th}} d^3 r \right. \\ &\quad \left. + 18 \int n_{\text{th}}^2 n_0 d^3 r + 6 \int n_{\text{th}}^3 d^3 r \right] - N/\tau \end{aligned} \quad (2)$$

where we have taken into account wavefunction symmetrisation (Ref. [30]), $L = 1.8 \times 10^{-29} \text{ cm}^6 \text{ s}^{-1}$ is the three-body decay coefficient taken from Ref. [26] and $\tau = 2 \text{ s}$ is the e^{-1} decay time for one-body (background) loss calibrated against dilute clouds trapped within the array. We assume that thermal equilibrium is maintained due to the high elastic collision rate and we treat the cloud temperature as a constant parameter during decay. Fitting the numerical solution of Eq. (2) to each decay curve provides the initial N and T . For all sets of experimental parameters the three-body decay curves are measured between 6 and 15 times and fit independently to reduce noise and estimate statistical uncertainties. For the intermediate temperatures ($\nu_f = 8300 \text{ kHz}$ and $\nu_f = 8500 \text{ kHz}$ datasets) we compare the results of both three-body decay and rf-spectroscopy measurements to calibrate systematic uncertainties such as the effective absorption cross-section used to determine N from absorption images.

Transporting atoms with external fields

The atoms are trapped in local minima of the total magnetic field strength. The total magnetic vector field is the superposition of fields from the chip and the external field. Thus the position of field minima depends also on the external field. By applying time-varying, external uniform fields in a cyclic fashion we can move the minima across the chip

surface. The shifting direction is reversed by simply reversing the order of the applied fields. Details of this calculation, as well as restrictions to where one can or cannot move the atoms can be found in Ref. [29].

* Electronic address: whitlock@science.uva.nl

- [1] Cirac, J. I. & Zoller, P. A scalable quantum computer with ions in an array of microtraps. *Nature* **404**, 579–581 (2000).
- [2] Deutsch, I. H., Brennen, G. K. & Jessen, P. S. Quantum computing with neutral atoms in an optical lattice. *Fortschr. Phys* **48**, 925–943 (2000).
- [3] Hänsel, W., Hommelhoff, P., Hänsch, T. W. & Reichel, J. Bose-Einstein condensation on a microelectronic chip. *Nature* **413**, 498–501 (2001).
- [4] Ott, H., Fortágh, J., Schlotterbeck, G., Grossmann, A. & Zimmermann, C. Bose-Einstein condensation in a surface microtrap. *Phys. Rev. Lett.* **87**, 230401 (2001).
- [5] Kielpinski, D., Monroe, C. & Wineland, D. J. Architecture for a large-scale ion-trap quantum computer. *Nature* **417**, 709–711 (2002).
- [6] Seidelin, S. *et al.* Microfabricated surface-electrode ion trap for scalable quantum information processing. *Phys. Rev. Lett.* **96**, 253003 (2006).
- [7] Stick, D. *et al.* Ion trap in a semiconductor chip. *Nature Phys.* **2**, 36–39 (2006).
- [8] Hensinger, W. K. *et al.* T-junction ion trap array for two-dimensional ion shuttling, storage, and manipulation. *Appl. Phys. Lett.* **88**, 034101 (2006).
- [9] Greiner, M., Mandel, O., Esslinger, T., Hänsch, T. W. & Bloch, I. Quantum phase transition from a superfluid to a Mott insulator in a gas of ultracold atoms. *Nature* **415**, 39–44 (2002).
- [10] Schrader, D. *et al.* Neutral atom quantum register. *Phys. Rev. Lett.* **93**, 150501 (2004).
- [11] Nelson, K. D., Li, X. & Weiss, D. S. Imaging single atoms in a three-dimensional array. *Nature Phys.* **3**, 556–560 (2007).
- [12] Peil, S. *et al.* Patterned loading of a Bose-Einstein condensate into an optical lattice. *Phys. Rev. A* **67**, 051603 (2003).
- [13] Bergamini, S. *et al.* Holographic generation of microtrap arrays for single atoms by use of a programmable phase modulator. *J. Opt. Soc. Am. B* **21**, 1889–1894 (2004).
- [14] Dumke, R. *et al.* Micro-optical realization of arrays of selectively addressable dipole traps: A scalable configuration for quantum computation with atomic qubits. *Phys. Rev. Lett.* **89**, 097903 (2002).
- [15] Reichel, J. Microchip traps and Bose-Einstein condensation. *Appl. Phys. B* **75**, 469–487 (2002).
- [16] Folman, R., Krüger, P., Schmiedmayer, J., Denschlag, J. & Henkel, C. Microscopic atom optics: from wires to an atom chip. *Advances in Atomic, Molecular and Optical Physics* **48**, 263–356 (2002).
- [17] Sinclair, C. D. J. *et al.* Bose-Einstein condensation on a permanent-magnet atom chip. *Phys. Rev. A* **72**, 031603R (2005).
- [18] Hall, B. V., Whitlock, S., Scharnberg, F., Hannaford, P. & Sidorov, A. A permanent magnetic film atom chip for Bose-Einstein condensation. *J. Phys. B: At. Mol. Opt.*

- Phys.* **39**, 27–36 (2006).
- [19] Fernholz, T., Gerritsma, R., Whitlock, S., Barb, I. & Spreuw, R. J. C. Fully permanent magnet atom chip for Bose-Einstein condensation. *Phys. Rev. A* **77**, 033409 (2008).
- [20] Treutlein, P., Hommelhoff, P., Steinmetz, T., Hänsch, T. W. & Reichel, J. Coherence in microchip traps. *Phys. Rev. Lett.* **92**, 203005 (2004).
- [21] Calarco, T. *et al.* Quantum gates with neutral atoms: Controlling collisional interactions in time-dependent traps. *Phys. Rev. A* **61**, 022304 (2000).
- [22] Jaksch, D. *et al.* Fast quantum gates for neutral atoms. *Phys. Rev. Lett.* **85**, 2208–2211 (2000).
- [23] Gerritsma, R. *et al.* Lattice of microtraps for ultracold atoms based on patterned magnetic films. *Phys. Rev. A* **76**, 033408 (2007).
- [24] Singh, M. *et al.* One dimensional lattice of permanent magnetic microtraps for ultracold atoms on an atom chip. *J. Phys. B: At. Mol. Opt. Phys.* **41**, 065301 (2008).
- [25] Burt, E. A. *et al.* Coherence, correlations, and collisions: What one learns about Bose-Einstein condensates from their decay. *Phys. Rev. Lett.* **79**, 337 (1997).
- [26] Söding, J. *et al.* Three-body decay of a rubidium Bose-Einstein condensate. *Appl. Phys. B* **69**, 257–261 (1999).
- [27] Hijmans, T. W., Kagan, Y., Shlyapnikov, G. V. & Walraven, J. T. M. Bose condensation and relaxation explosion in magnetically trapped atomic hydrogen. *Phys. Rev. B* **48**, 12886 (1993).
- [28] Meek, S. A., Bethlem, H. L., Conrad, H. & Meijer, G. Trapping molecules on a chip in traveling potential wells *arXiv:0801.2943* (2008).
- [29] Gerritsma, R. & Spreuw, R. J. C. Topological constraints on magnetostatic traps. *Phys. Rev. A* **74**, 043405 (2006).
- [30] Kagan, Y., Svistunov, B. V. & Shlyapnikov, G. V. Effect of Bose condensation on inelastic processes in gases. *JETP Lett.* **42**, 209–212 (1985).
- Acknowledgments:** We would like to thank M. S. Golden, H. B. van Linden van den Heuvell and N. J. van Druten for helpful discussions and careful reading of the manuscript. We thank J.-U. Thiele (Hitachi San Jose Research Center) and the magnetic materials group of J. B. Goedkoop (U. of Amsterdam) for developing the FePt films. The chips were patterned using the facilities of the Amsterdam *nanoCenter*. This work is part of the research programme of the ‘Stichting voor Fundamenteel Onderzoek der Materie (FOM)’, which is financially supported by the ‘Nederlandse Organisatie voor Wetenschappelijk Onderzoek (NWO)’. It was also supported by the EU under contract MRTN-CT-2003-505032.
- Competing financial interests:** The authors declare that they have no competing financial interests.